Journal of Materials Chemistry A

RSC Publishing

PAPER

View Article Online
View Journal | View Issue

Facile synthesis of a Co_3O_4–carbon nanotube composite and its superior performance as an anode material for Li-ion batteries

Cite this: *J. Mater. Chem. A*, 2013, **1**, 1141

Linhai Zhuo,[ac] Yingqiang Wu,[acd] Jun Ming,[ac] Lingyan Wang,[acd] Yancun Yu,[ac] Xinbo Zhang*[b] and Fengyu Zhao*[ac]

In this work, we report a facile method for the synthesis of a Co_3O_4–functionalized carbon nanotube (Co_3O_4–f-CNT) composite *via* the growth of Co_3O_4 nanoparticles on the surface of functionalized carbon nanotubes (f-CNTs) by thermal decomposition of cobalt nitrate hexahydrate in ethanol. The composite consists of 13% carbon nanotubes and 87% Co_3O_4 nanoparticles by weight, and all the Co_3O_4 particles grew compactly along the carbon nanotube axis with a highly uniform dispersion. When used as an anode material for rechargeable lithium ion batteries, the composite manifested high capacities and excellent cycling performance at high and low current rates. The discharge capacity was 719 mA h g^{-1} at the 2nd cycle and 776 mA h g^{-1} at the 100th cycle. Even at a current density of 1 A g^{-1}, the specific capacity still remained at about 600 mA h g^{-1}. This superior electrochemical performance was attributed to the unique nanostructure of the composite. Because almost all of the Co_3O_4 nanoparticles were immobilized on the surface of f-CNTs, physical aggregation of nanoparticles was avoided during the charge–discharge processes. Furthermore, the good mechanical flexibility of f-CNTs can readily alleviate the massive volume expansion/shrinkage associated with a conversion reaction electrode. Finally, f-CNTs are highly conductive matrices for electrons due to their high conductivity, which can shorten the diffusion path for electrons.

Received 12th September 2012
Accepted 9th November 2012

DOI: 10.1039/c2ta00284a

www.rsc.org/MaterialsA

Introduction

Energy storage is becoming more and more important due to the ever-increasing concerns about limited energy supply, air pollution and global warming.[1–4] Among the various electrochemical storage technologies, rechargeable lithium ion batteries (LIBs), which can deliver high energy density and power density with good cycle ability, are considered promising candidates.[1] However, for some special applications, such as vehicles and large energy-storage devices, it is necessary to dramatically increase their capacity and cyclability. In recent years, considerable efforts have been devoted to the development of new electrode materials with higher gravimetric and volumetric capacities. For this purpose, 3d transition metal oxides have been studied widely as possible alternatives to carbonaceous anode materials because they exhibit capacities 2–3 times larger than graphite.[5–13] However, the practical application of these metal oxides as anode materials is hampered due to their lower electronic and ionic conductivities, large volume changes, and polarisation during cycling.[14,15]

Synthesizing nanostructured carbon–metal oxide hybrid materials is an effective way to circumvent these problems. It can not only buffer the internal volume changes during cycling but also enhance the electronic conductivity of the composites.[16–25] As a member of carbon family, carbon nanotubes (CNTs) are one of the best choices for combination with active materials in view of their facile fabrication, high aspect ratio, strong mechanical strength, and sufficient electrical and ion conductivity.[26,27] Therefore, intensive research has been devoted to developing CNT-based composites with heterogeneous nanostructures, such as $Li_4Ti_5O_{12}$–CNT,[28] SnO_2–CNT,[15,29,30] Fe_3O_4–CNT,[19] CuO–CNT,[31] MnO_2–CNT,[32–34] and Co_2SnO_4–CNT.[33] However, there have been only a few reports on the preparation of Co_3O_4–CNT composites.[17,18] Gao and Shan synthesised a Co_3O_4–CNT composite by *in situ* coating of CNTs with Co_3O_4 nanocrystals.[17] As claimed, the capacity fading and the stability toward electrochemical cycling were greatly improved compared with these Co_3O_4 nanocrystals. In addition, Wang *et al.* synthesised Co_3O_4–CNT composites by a hydrothermal synthesis method.[18] The obtained Co_3O_4–CNT composite

[a]*State Key Laboratory of Electroanalytical Chemistry, Changchun Institute of Applied Chemistry, Chinese Academy of Sciences, Changchun, 130022, P. R. China. E-mail: zhaofy@ciac.jl.cn*

[b]*State Key Laboratory of Rare Earth Resource Utilizations, Changchun Institute of Applied Chemistry, Chinese Academy of Sciences, Changchun, 130022, P. R. China. E-mail: xbzhang@ciac.jl.cn*

[c]*Laboratory of Green Chemistry and Process, Changchun Institute of Applied Chemistry, Chinese Academy of Sciences, Changchun 130022, China. Fax: +86-431-85262410; Tel: +86-431-85262410*

[d]*University of the Chinese Academy of Sciences, Beijing 100049, China*

exhibited an initial lithium storage capacity of 1250 mA h g^{-1} and a capacity of 530 mA h g^{-1} over 100 cycles at a current density of 0.1 C. However, the rate performances of these Co_3O_4–CNT composites were not involved. Further improvement in their rate performance is still needed in the near future. Furthermore, the reported methods always required surfactants, template agents or precipitators, which complicated the subsequent separation process. This is one of the critical factors that restrict the realization of these CNT-based hybrid materials on a large scale in the commercial market.[14,23]

In our previous work, CNTs were functionalized through a simple steaming method.[35] During the steaming process, large amounts of functional groups are introduced onto the surface of nanotubes and thus enhance the ability of the carbon nanotubes to immobilize guest components. In this work, the functionalized carbon nanotubes (f-CNTs) are used to synthesize a Co_3O_4–f-CNT composite by the thermal decomposition of cobalt nitrate hexahydrate in ethanol. As a result, Co_3O_4 nanoparticles were compactly coated onto the surfaces of f-CNTs with a uniform dispersion due to the abundant functional groups and edges on the f-CNTs. The advantages of this method include simple operation, low cost, little pollution, and amenability to large-scale synthesis. When used as anode materials for rechargeable LIBs, the CNT–f-Co_3O_4 composite manifested high capacities and excellent cycling performance at multiple current rates.

Experimental section

Reagents and materials

The multiwalled carbon nanotubes (CNTs, length 5–15 μm, diameter 40–60 nm, purity >98%) were purchased from Shenzhen Nanotech Port Co., Ltd. Concentrated HNO_3 (65–68 wt%) and cobalt nitrate hexahydrate [$Co(NO_3)_2 \cdot 6H_2O$] were purchased from Sinopharm Chemical Reagent Beijing Co. Ltd. and used directly.

Methods

Pristine CNTs (p-CNTs) were purified with 6 M HNO_3 in an ultrasonic bath for 30 minutes, followed by washing with high purity water and filtration. F-CNTs were prepared using our previous method.[35] The as-prepared f-CNTs (10 mg) were well dispersed in 10 ml of an ethanol solution of $Co(NO_3)_2 \cdot 6H_2O$ (0.3 g) in a glass bottle under ultrasonic treatment for 30 minutes. Then, the dense colloidal solution was transferred into an autoclave vessel (50 ml), which was sealed and placed into an oven at 120 °C for 24 h. The autoclave was then cooled to room temperature, and the resulting product was centrifuged and washed repeatedly with deionised water and ethanol, followed by drying under vacuum at 80 °C for 12 h. Next, the samples were heat-treated at 400 °C with a heating rate of 5 °C min^{-1} and held for 4 h under argon. The Co_3O_4–f-CNT composite was thus obtained. For comparison, p-CNTs were used to synthesise a Co_3O_4–p-CNT composite according to the same procedure.

Characterizations

The phase structures were characterised with X-ray diffraction [XRD, Bruker D8 Advance diffractometer using Cu K_α (λ = 1.5418 Å)]. The morphology of the materials was analysed on a scanning electron microscope (SEM Hitachi S-4800). Transmission electron microscope (TEM) images were recorded on a Tecnai G20 operating at 200 kV for detailed sample microstructure information. Thermal gravimetric analysis (TGA) was carried out using a TGA 2050 thermogravimetric analyser. X-ray photoelectron spectra (XPS) were recorded on a PHI Quantera SXM spectrometer with an Al K_α = 280.00 eV excitation source, and binding energies were calibrated by referencing the C1s peak (284.5 eV) to reduce the sample charge effect.

Electrochemical characterization

The electrochemical tests were measured using two-electrode 2025-type coin cells assembled in an argon-filled glove box. Lithium sheets served as the counter electrode and reference electrode, and a polypropylene film (Celgard-2300) was used as a separator. The electrolyte was a 1.0 M $LiPF_6$ solution in a mixture of EC–DMC (1 : 1 by volume). The working electrodes were prepared using a slurry coating procedure. The slurry consisted of 80 wt% active materials, 10 wt% acetylene black and 10 wt% polyvinylidene fluorides dissolved in *N*-methyl-2-pyrrolidinone. This slurry was spread on copper foil, which acted as a current collector. The electrodes were dried at 120 °C for 4 h in air and at 120 °C under vacuum for another 12 h. The electrode disks (d = 12 mm) were pressed, and weighed accurately by an electronic balance. The mass error of the active material is 0.01 mg. The total weight of the active material loading on the collectors is controlled in the range of 1–2 mg. Galvanostatic charge–discharge cycles were carried out on a battery tester between 0.01 and 3.00 V at various current densities on a LAND CT2001A cell test instrument (Wuhan Kingnuo Electronic Co., China). For comparison, bare f-CNTs, p-CNTs and commercial Co_3O_4 were tested under the same experimental conditions. The specific capacity was calculated based on the whole mass of the composites, specifically the sum mass of Co_3O_4 and CNTs for the Co_3O_4–CNT composites.

Results and discussion

Because of the inert walls of the p-CNTs, it is difficult to deposit foreign materials on them directly. Therefore, p-CNTs usually need oxidative pre-treatment or modification with surfactants to generate functional groups on the sidewalls.[36] As shown in Fig. 1a, the p-CNTs have a smooth outer surface with diameters of 40–60 nm and are several micrometres in length. After chemical etching with acid vapour (Fig. 1b and c), the length of the f-CNTs was reduced to hundreds of nanometres, and the rough surfaces indicate an increase in the number of edges in the graphite layers and the formation of lateral defects. The TEM images (Fig. 1d) showed that some CNTs were etched deeply, with holes in the walls. The number of functional groups on the surfaces of CNTs is one of the key factors affecting the load quality of foreign materials. To determine the relative levels of oxidation of f-CNTs, X-ray photoelectron spectroscopy (XPS) was carried out (Fig. 1e and f). The C1s spectra of f-CNTs and p-CNTs were compared by deconvolution

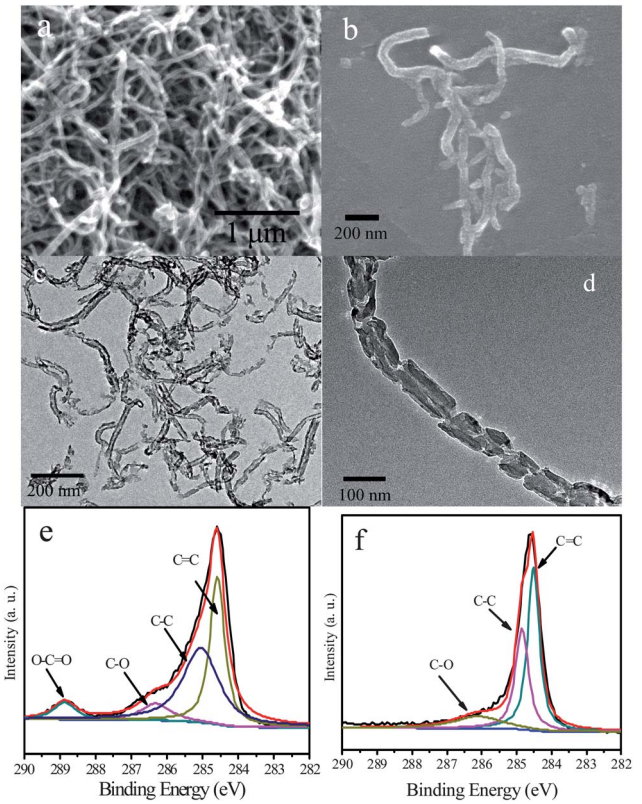

Fig. 1 Typical SEM images of (a) p-CNTs and (b) f-CNTs. (c) Typical TEM image of f-CNTs. (d) A magnified TEM image of an f-CNT. C1s spectra of (e) f-CNTs and (f) p-CNTs.

(Multipack software, version 7.0). The C1s spectra of f-CNTs (Fig. 1e) could be deconvoluted into four peaks that corresponded to carbon sp^2 (C=C, 284.5 eV), carbon sp^3 (C–C, 285.1 eV), epoxy/hydroxyls (C–O, 286.2 eV), and carboxylates (O–C=O, 288.9 eV). In contrast, the C1s spectra of p-CNTs (Fig. 1f) could only be deconvoluted into carbon sp^2 (C=C, 284.5 eV), carbon sp^3 (C–C, 285.1 eV) and epoxy/hydroxyls (C–O, 286.2 eV).[36] This observation suggested that the surface of the f-CNTs generated large amounts of acidic groups after oxidative treatment. Because carboxyl groups have the highest affinity for metal ions in a wide range of pH,[37] the f-CNTs could retain foreign materials better after oxidative treatment.

Herein, the two types of CNTs were used to synthesise Co_3O_4–CNT composites *via* a simple solvothermal method, and their electrochemical performances were studied and compared. The overall crystal structure and phase purity of the Co_3O_4–f-CNT and Co_3O_4–p-CNT composites were identified by XRD. As shown in Fig. 2, all of the resolved diffraction peaks were well indexed to that of cubic spinel Co_3O_4 (Joint Committee on Powder Diffraction Standards (JCPDS) card no. 42-1467), indicating the high purity of the obtained samples.

The morphologies of the Co_3O_4–CNT composites are studied by SEM and TEM. As shown in Fig. 3a, almost all of the Co_3O_4 nanoparticles were coated onto the surface of the f-CNTs. Notably, these spherical particles were distributed along the axis of the carbon nanotubes with good adherence to the walls

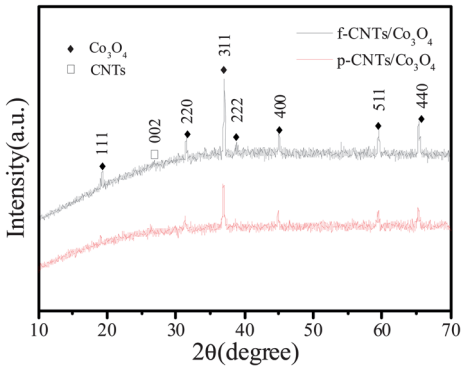

Fig. 2 XRD patterns of the Co_3O_4–f-CNT and Co_3O_4–p-CNT composites.

of f-CNTs. The nanoparticles were approximately 150–300 nm in diameter. The TEM image of the Co_3O_4–f-CNT composite shown in Fig. 3c revealed that all the Co_3O_4 NPs were anchored on the external surfaces of the f-CNTs. The HRTEM image of the cross-section of the composite (Fig. 3d) revealed that there were two types of lattice fringes with a lattice spacing of 0.29 and 0.34 nm, which corresponded to the (220) plane of Co_3O_4 nanoparticles and the (002) plane of CNTs, respectively. The formation of such a compact and uniform Co_3O_4–f-CNT composite should be ascribed to the abundant functional groups and lateral defects of the f-CNTs. By contrast, the morphologies of the Co_3O_4–p-CNT composite showed that the Co_3O_4 particles were dispersed freely on the Co_3O_4–p-CNT sample with an average diameter of 300–500 nm without intimate contact with the p-CNTs (Fig. 3b and e). To understand how the f-CNTs influenced the deposition of Co_3O_4 on their surface, we also investigated the decomposition of cobalt nitrate in ethanol under the same conditions without CNTs. In this case, the colour of the solution was still pink after 24 hour heating in the autoclave, indicating that the cobalt nitrate was not completely decomposed. The present study suggests that free cobalt nitrate is decomposed slowly in solution. In the presence of CNTs, cobalt ions can first randomly adsorb onto the surface of CNTs as nucleation sites.

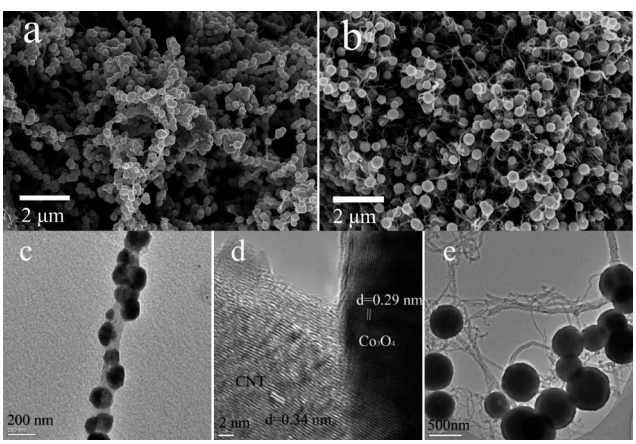

Fig. 3 SEM images of (a) Co_3O_4–f-CNT and (b) Co_3O_4–p-CNT composites. (c) TEM image of a Co_3O_4–f-CNT composite. (d) HRTEM image of the cross-section of the Co_3O_4–f-CNT composite. (e) TEM image of a Co_3O_4–p-CNT composite.

During synthesis, these residual cobalt ions in solution are adsorbed continuously onto the nucleation sites and slowly crystallise to Co_3O_4 nanoparticles *in situ* at a low temperature. Compared with p-CNTs, f-CNTs provide more nucleation sites due to their abundant functional groups and lateral defects, which should lead to the formation of smaller particles and good adherence.

To quantify the amount of CNTs in the composites, TGA analysis of the Co_3O_4–f-CNT and Co_3O_4–p-CNT composites was carried out in air. The samples were heated from room temperature to 800 °C at a rate of 10 °C min^{-1}. Fig. 4 shows the resulting TGA curves of the Co_3O_4–f-CNT and Co_3O_4–p-CNT composites. As seen, the composites showed a rapid mass loss between 350 and 600 °C, which is ascribed to the oxidation of CNTs because the bare Co_3O_4 was stable in this temperature range. Based on this analysis, the amounts of CNTs in the Co_3O_4–f-CNT and Co_3O_4–p-CNT composites were estimated to be 13% and 14%, respectively.

The electrochemical performance of CNTs was closely related to their structure, morphology, and disorder. To identify all the electrochemical reactions of f-CNTs and p-CNTs, cyclic voltammograms (CVs) were conducted on the cells made from the two types of CNTs for two cycles at room temperature. Both materials were studied in the potential range of 0.01–3.0 V *vs.* Li/Li^+ at a scan rate of 0.2 mV s^{-1}. The first cathodic scan of both types of CNTs was characterised by peaks in the range of 0.5–0.8 V. However, no peaks were observed after the second discharge cycle. These peaks were attributed to electrolyte decomposition and formation of a solid-electrolyte-interface (SEI) layer.[38,39] In the first anodic scan, peaks at 0.2 V and 1.25 V were observed for both types of CNTs, and attributed to the extraction of Li ions from the graphitic layers and the inner channels of the CNTs, respectively.[39]

To compare their Li-ion storage ability, charge–discharge curves for p-CNTs and f-CNTs at a current density of 200 mA g^{-1} are shown in Fig. 5c and d. The plotted data show the first two cycles corresponding to the discharge and charge processes. During discharge, the potential dropped rapidly to approximately 0.8 V, and a shoulder was observed only in the first cycle. The shoulder appeared at approximately 0.8 V in the discharge curve from the first cycle could be related to the formation of an SEI layer on the CNT surface. These results were also observed in the CVs of the composites. The reversible capacities of f-CNTs and p-CNTs were 478 and 231 mA h g^{-1}, respectively. The increased reversible capacity of f-CNTs should be mainly attributed to the enhanced extraction of Li ions from the graphitic layers because the peak at 0.2 V is more pronounced for f-CNTs, which indicates that more Li ions are reversibly extracted from f-CNTs compared to p-CNTs.[38,39]

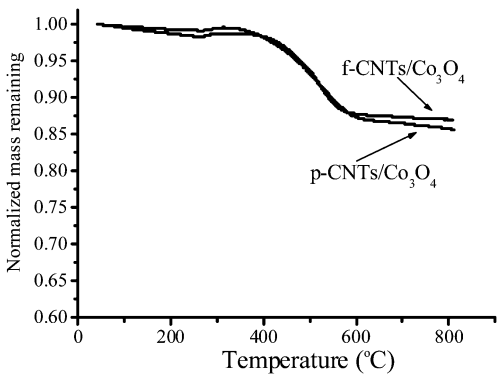

Fig. 4 TGA curves of Co_3O_4–f-CNT and Co_3O_4–p-CNT composites heated in air.

To examine the electrochemical properties of these composites, CVs were conducted with Co_3O_4–f-CNT and Co_3O_4–p-CNT as anodes based on the half cell configuration. Fig. 6a and b show the CVs of the Co_3O_4–f-CNT and Co_3O_4–p-CNT composites. Both of them were studied in the potential range of 0.01–3.0 V *vs.* Li/Li^+ at a scan rate of 0.2 mV s^{-1}. The first cathodic scan of the Co_3O_4–f-CNT and Co_3O_4–p-CNT composites presented an irreversible reduction peak at ~0.8 V attributed to electrolyte decomposition and formation of an SEI layer. After the first scan, the CV pattern of the Co_3O_4–f-CNT composites showed two cathodic peaks at ~1.1 V and ~0.8 V, and the corresponding anodic peaks at ~2.0 V and ~2.5 V. The pair of cathodic and anodic peaks likely originated from the redox reaction $Co^{3+/2+}/Co^0$. Specifically, Co_3O_4 has a normal spinel structure with Co^{2+} ions and Co^{3+} ions in a cubic close packed lattice of oxide anions, so the reduction–oxidation reaction of $Co^{3+/2+}/Co^0$ is a complex multi-step process.[11] However, the pair of cathodic and anodic peaks was not clearly visible in the Co_3O_4–p-CNT electrode. This behaviour meant that f-CNTs significantly improved the electrochemical activity of Co_3O_4 during the cyclic process. Furthermore, the Co_3O_4–f-CNT cell showed nicely overlapping redox peaks upon extended scans. This indicated an improved electrochemical stability of the synthesised Co_3O_4–f-CNT material.[11]

Both Co_3O_4 and CNTs were able to react with lithium ions for reversible lithium storage. It has been reported that one mole of Co_3O_4 has the ability to react with eight moles of Li ions through the reaction: $Co_3O_4 + 8Li^+ + 8e \leftrightarrow 4Li_2O + 3Co$. Based on this reaction, the theoretical capacity of Co_3O_4 could be calculated as 895 mA h g^{-1}.[22] In addition, the largest reversible capacity of the f-CNTs was 478 mA h g^{-1}. Therefore, the theoretical capacity of the Co_3O_4–f-CNT composites was 840 mA h g^{-1} (478 mA h g^{-1} × 0.13 + 895 mA h g^{-1} × 0.87).[16] The charge–discharge curves for the Co_3O_4–f-CNT and Co_3O_4–p-CNT composites at a current density of 200 mA g^{-1} are shown in Fig. 6. The plotted data show the 1st, 2nd, and 60th cycles of discharge and charge. In the first discharge step, both of the samples exhibited long voltage plateaus at 1.0 V followed by a sloping curve down to 0.01 V, which is typical of voltage trends for Co_3O_4 electrodes.[16,40,41] The first discharge and charge capacities of Co_3O_4–f-CNTs were 943 mA h g^{-1} and 639 mA h g^{-1}, respectively. The Co_3O_4–f-CNT composite exhibited a discharge capacity of 719 mA h g^{-1} at the 2nd cycle and 823 mA h g^{-1} at the 60th cycle. The Coulombic efficiency rose from 67.7% at the 1st cycle to 92% at the 2nd cycle and 99.4% at the 60th cycle. The initial Coulombic efficiency (67.7%) of the Co_3O_4–f-CNTs was comparable to Co_3O_4–carbon composite nanowires (66.8%),[42] Co_3O_4–graphene composites (68.6%),[41] mesoporous carbon–Co_3O_4 (55%),[43] nanoparticles (55.2%),[44] nanotubes (58.8%),[44] and nanorods (57.8%).[44] The low Coulombic

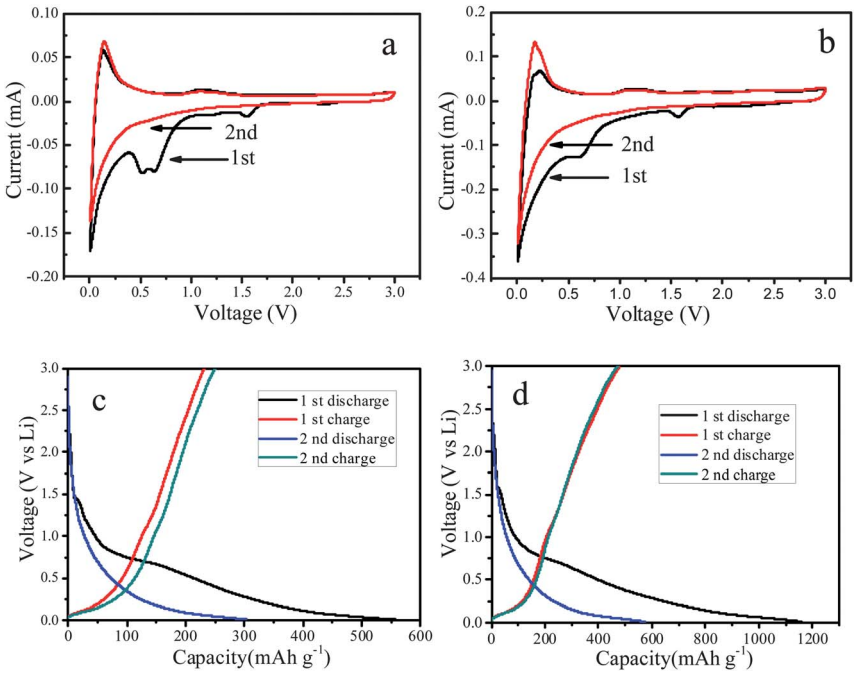

Fig. 5 Cyclic voltammograms (CVs) of p-CNTs (a) and f-CNTs electrodes (b) at a scan rate of 0.2 mV s^{-1} during the first two cycles. The first two charge–discharge voltage profiles of (c) p-CNTs and (d) f-CNTs.

efficiencies are normally attributed to irreversible reactions occurring during the first discharge, which can cause an inevitable loss of anode materials.[16,21,45] In contrast, the first discharge and charge capacities of Co_3O_4–p-CNT were 838 mA h g^{-1} and 629 mA h g^{-1}. After 60 cycles, the Co_3O_4–p-CNT electrode only retained a capacity of 424 mA h g^{-1}. The rapid decrease in capacity of the CNT–p-Co_3O_4 composites was likely the result of non-intimate contact between p-CNTs and Co_3O_4 particles.

For the typical life time study, the cells made from Co_3O_4–f-CNT, Co_3O_4–p-CNT, f-CNTs, p-CNTs, and Co_3O_4 (commercial) were discharged and charged at a current density of 200 mA g^{-1} up to 100 cycles. Fig. 7a shows the cycling behaviour of the Co_3O_4–f-CNT composite. The cell retained a reversible capacity

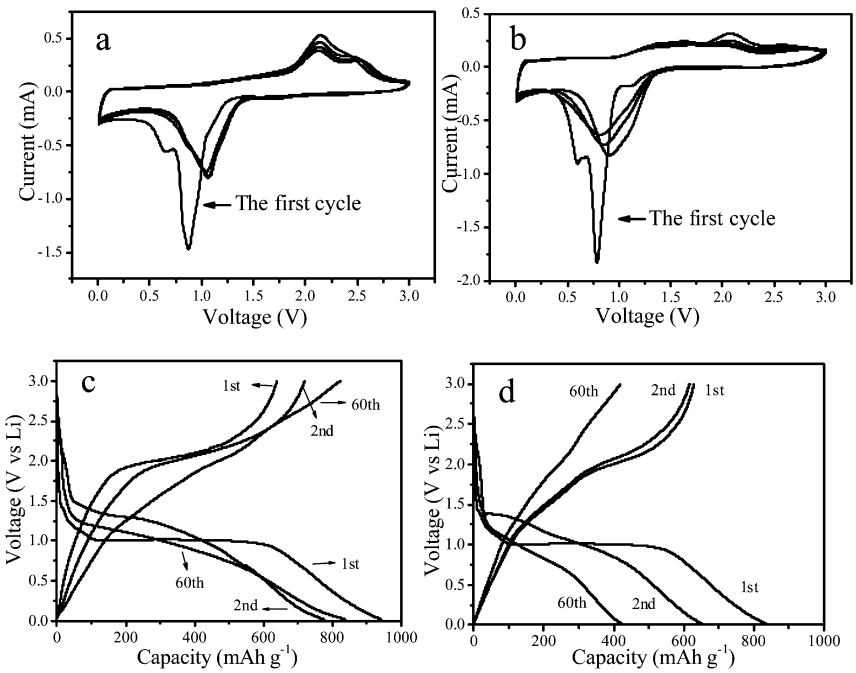

Fig. 6 Typical cyclic voltammograms of (a) Co_3O_4–f-CNT and (b) Co_3O_4–p-CNT at a sweep rate of 0.2 mV s^{-1}. The 1st, 2nd, and 60th charge–discharge voltage profiles of Co_3O_4–f-CNT (c) and Co_3O_4–p-CNT composite electrodes (d) at a current density of 200 mA g^{-1}.

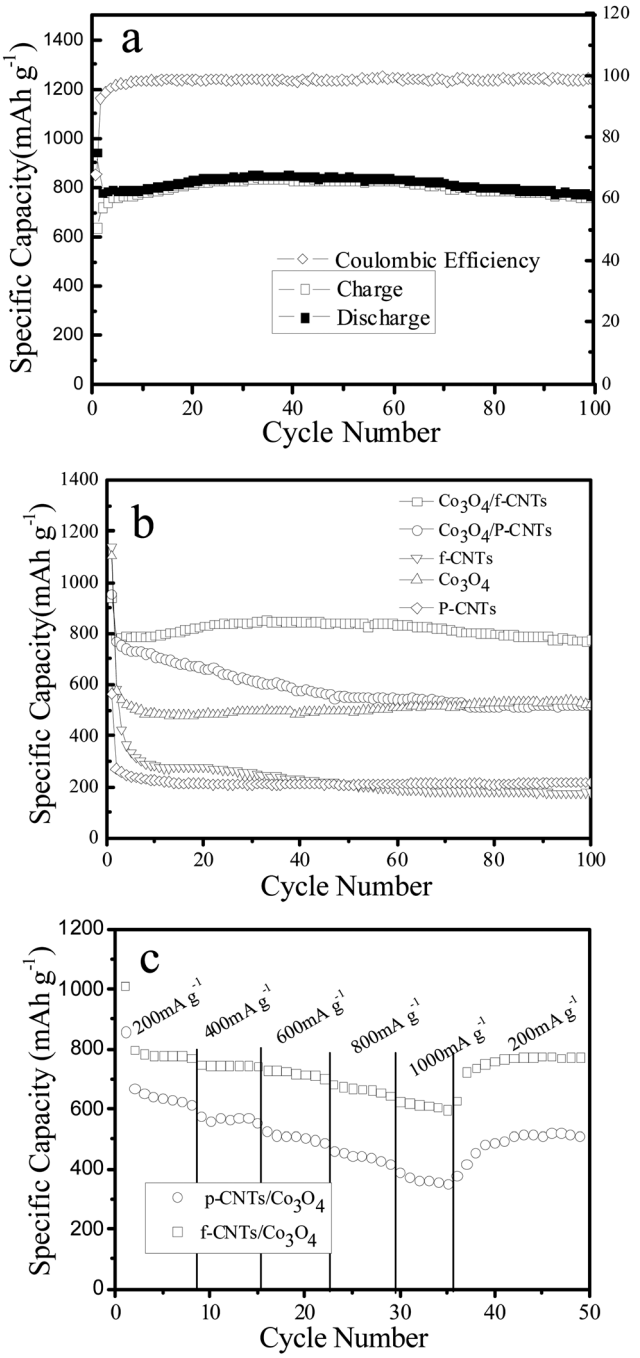

Fig. 7 (a) Cycling behaviour of the Co_3O_4–f-CNT composite at a current density of 200 mA g^{-1}. (b) Cycling behaviours of Co_3O_4–f-CNT, Co_3O_4–p-CNT, f-CNTs, p-CNTs, and Co_3O_4 (commercial) at a current density of 200 mA g^{-1}. (c) Discharge capacity *vs.* cycle number of Co_3O_4–f-CNT and Co_3O_4–p-CNT composite electrodes at various current densities.

of 776 mA h g^{-1} with a Coulombic efficiency of 99.1% after 100 cycles. It should be noted that the reversible capacity of the Co_3O_4–f-CNT composite slightly increased with higher cycling numbers and reached ~850 mA h g^{-1} after 30 cycles. This behaviour was attributed to the gradual activation of the electrode in the first several cycles.[46] A control experiment was carried out with Co_3O_4–p-CNT composites and provided a much lower discharge capacity and poor cyclability relative to Co_3O_4–f-CNT composites (Fig. 7b). When the Co_3O_4–f-CNT composite was compared with bare CNTs and commercial Co_3O_4, its high capacity was even more evident. To further investigate the electrochemical performances of Co_3O_4–f-CNT and Co_3O_4–p-CNT composites, the charge–discharge measurements were also carried out at various current densities. As shown in Fig. 7c, the Co_3O_4–f-CNT composite also presented good rate performance, even at a current density of 1 A g^{-1}, and the specific capacity of the Co_3O_4–f-CNT composite was as high as 600 mA h g^{-1}. However, the capacity of the Co_3O_4–p-CNT composite dropped dramatically to 350 mA h g^{-1} at the same current density. If the current changed from 1 A g^{-1} to 200 mA g^{-1}, the specific capacity of the Co_3O_4–f-CNT composite gradually returned to ~770 mA g^{-1}, indicating high cycling stability.

Compared with the reported Co_3O_4–CNT composites, the Co_3O_4–f-CNT composite exhibits considerably better electrochemical behaviors.[17,18] This improvement was attributed to its unique nanostructure. First, the abundant functional groups and lateral defects on f-CNTs provided more nucleation sites for the growth of Co_3O_4 nanoparticles, forming compact and highly dispersed Co_3O_4 nanoparticles on the surfaces of the CNTs with high loading. Second, the solvent and low temperature are also important to hold the decomposition at a low rate to avoid particle formation in solution. On the other hand, if the nucleation was faster, some nanoparticles would crystallise in solution, and either adsorb onto the as-originated particles or agglomerate in solution,[47] which would lead to a decreased binding or a loss of contact between individual nanoparticles and CNTs.

Conclusions

In summary, we have developed a facile method to immobilize Co_3O_4 particles on f-CNTs to form a Co_3O_4–f-CNT composite. An in-depth electrochemical investigation revealed that the Co_3O_4–f-CNT composite had a high reversible capacity, good cycling stability and excellent rate capability than that of Co_3O_4–p-CNT. Because almost all of the Co_3O_4 nanoparticles were immobilized on the surface of the f-CNTs, physical aggregation of nanoparticles was avoided during the charge–discharge cycles. The intimate contact between the f-CNTs and Co_3O_4 nanoparticles afforded a facile electron transport to ensure electrochemical activity. Furthermore, the good mechanical flexibility of the f-CNTs readily adsorbed the massive volume expansion associated with a conversion reaction electrode. The strategy described in this paper is very simple and could be extended to the synthesis of other metal oxide composites with f-CNTs for use as anode materials in LIBs.

Acknowledgements

This work was financially supported by the One Hundred Talent Program of CAS and NSFC (21273222).

Notes and references

1 M. Armand and J. M. Tarascon, *Nature*, 2008, **451**, 652.
2 P. G. Bruce, S. A. Freunberger, L. J. Hardwick and J.-M. Tarascon, *Nat. Mater.*, 2012, **11**, 19.
3 A. Manthiram, *J. Phys. Chem. Lett.*, 2011, **2**, 176.
4 M. G. Kim and J. Cho, *Adv. Funct. Mater.*, 2009, **19**, 1497.
5 Y. Zou and Y. Wang, *Nanoscale*, 2011, **3**, 2615.
6 Y. J. Mai, S. J. Shi, D. Zhang, Y. Lu, C. D. Gu and J. P. Tu, *J. Power Sources*, 2012, **204**, 155.
7 Y. Huang, X. L. Huang, J. S. Lian, D. Xu, L. M. Wang and X. B. Zhang, *J. Mater. Chem.*, 2012, **22**, 2844.
8 J. Su, M. Cao, L. Ren and C. Hu, *J. Phys. Chem. C*, 2011, **115**, 14469.
9 G. M. Zhou, D. W. Wang, F. Li, L. L. Zhang, N. Li, Z. S. Wu, L. Wen, G. Q. Lu and H. M. Cheng, *Chem. Mater.*, 2010, **22**, 5306.
10 L. W. Ji, Z. K. Tan, T. R. Kuykendall, S. Aloni, S. D. Xun, E. Lin, V. Battaglia and Y. G. Zhang, *Phys. Chem. Chem. Phys.*, 2011, **13**, 7139.
11 N. Jayaprakash, W. D. Jones, S. S. Moganty and L. A. Archer, *J. Power Sources*, 2012, **200**, 53.
12 Y. Q. Zou, J. Kan and Y. Wang, *J. Phys. Chem. C*, 2011, **115**, 20747.
13 B. J. Li, H. Q. Cao, J. Shao, M. Z. Qu and J. H. Warner, *J. Mater. Chem.*, 2011, **21**, 5069.
14 C. Xu, J. Sun and L. Gao, *J. Power Sources*, 2011, **196**, 5138.
15 J. Ren, J. Yang, A. Abouimrane, D. Wang and K. Amine, *J. Power Sources*, 2011, **196**, 8701.
16 B. Li, H. Cao, J. Shao, G. Li, M. Qu and G. Yin, *Inorg. Chem.*, 2011, **50**, 1628.
17 Y. Shan and L. Gao, *Chem. Lett.*, 2004, 1560.
18 G. Wang, X. Shen, J. Yao, D. Wexler and J.-h. Ahn, *Electrochem. Commun.*, 2009, **11**, 546.
19 C. M. Ban, Z. C. Wu, D. T. Gillaspie, L. Chen, Y. F. Yan, J. L. Blackburn and A. C. Dillon, *Adv. Mater.*, 2010, **22**, E145.
20 R. R. Bi, X. L. Wu, F. F. Cao, L. Y. Jiang, Y. G. Guo and L. J. Wan, *J. Phys. Chem. C*, 2010, **114**, 2448.
21 Y. Zhong, X. Wang, K. Jiang, J. Y. Zheng, Y. Guo, Y. Ma and J. Yao, *J. Mater. Chem.*, 2011, **21**, 17998.
22 H. Kim, D. H. Seo, S. W. Kim, J. Kim and K. Kang, *Carbon*, 2011, **49**, 326.
23 J. W. Lee, T. Ahn, D. Soundararajan, J. M. Ko and J. D. Kim, *Chem. Commun.*, 2011, **47**, 6305.
24 Y.-S. He, D.-W. Bai, X. Yang, J. Chen, X.-Z. Liao and Z.-F. Ma, *Electrochem. Commun.*, 2010, **12**, 570.
25 W. L. Yao, J. Yang, J. L. Wang and L. A. Tao, *Electrochim. Acta*, 2008, **53**, 7326.
26 F. F. Cao, Y. G. Guo, S. F. Zheng, X. L. Wu, L. Y. Jiang, R. R. Bi, L. J. Wan and J. Maier, *Chem. Mater.*, 2010, **22**, 1908.
27 G. Lota, K. Fic and E. Frackowiak, *Energy Environ. Sci.*, 2011, **4**, 1592.
28 L. F. Shen, C. Z. Yuan, H. J. Luo, X. G. Zhang, K. Xu and F. Zhang, *J. Mater. Chem.*, 2011, **21**, 761.
29 P. Wu, N. Du, H. Zhang, J. X. Yu and D. R. Yang, *J. Phys. Chem. C*, 2010, **114**, 22535.
30 L. Noerochim, J. Z. Wang, S. L. Chou, H. J. Li and H. K. Liu, *Electrochim. Acta*, 2010, **56**, 314.
31 J. Y. Xiang, J. P. Tu, J. Zhang, J. Zhong, D. Zhang and J. P. Cheng, *Electrochem. Commun.*, 2010, **12**, 1103.
32 J. Li, N. Wang, Y. Zhao, Y. Ding and L. Guan, *Electrochem. Commun.*, 2011, **13**, 698.
33 G. Wang, Z. Y. Liu and P. Liu, *Electrochim. Acta*, 2011, **56**, 9515.
34 A. L. M. Reddy, M. M. Shaijumon, S. R. Gowda and P. M. Ajayan, *Nano Lett.*, 2009, **9**, 1002.
35 J. Ming, Y. Wu, Y. Yu and F. Zhao, *Chem. Commun.*, 2011, **47**, 5223.
36 D. C. Marcano, D. V. Kosynkin, J. M. Berlin, A. Sinitskii, Z. Z. Sun, A. Slesarev, L. B. Alemany, W. Lu and J. M. Tour, *ACS Nano*, 2010, **4**, 4806.
37 K. Chojnacka, A. Chojnacki and H. Gorecka, *Chemosphere*, 2005, **59**, 75.
38 H. Shimoda, B. Gao, X. P. Tang, A. Kleinhammes, L. Fleming, Y. Wu and O. Zhou, *Phys. Rev. Lett.*, 2002, **88**, 015502.
39 X. X. Wang, J. N. Wang, H. Chang and Y. F. Zhang, *Adv. Funct. Mater.*, 2007, **17**, 3613.
40 X. Wang, X.-L. Wu, Y.-G. Guo, Y. Zhong, X. Cao, Y. Ma and J. Yao, *Adv. Funct. Mater.*, 2010, **20**, 1680.
41 Z.-S. Wu, W. Ren, L. Wen, L. Gao, J. Zhao, Z. Chen, G. Zhou, F. Li and H.-M. Cheng, *ACS Nano*, 2010, **4**, 3187.
42 P. Zhang, Z. P. Guo, Y. D. Huang, D. Z. Jia and H. K. Liu, *J. Power Sources*, 2011, **196**, 6987.
43 H.-j. Liu, S.-h. Bo, W.-j. Cui, F. Li, C.-x. Wang and Y.-y. Xia, *Electrochim. Acta*, 2008, **53**, 6497.
44 W. Y. Li, L. N. Xu and J. Chen, *Adv. Funct. Mater.*, 2005, **15**, 851.
45 J. Cabana, L. Monconduit, D. Larcher and M. R. Palacin, *Adv. Mater.*, 2010, **22**, E170.
46 L. Q. Tao, J. T. Zai, K. X. Wang, H. J. Zhang, M. Xu, J. Shen, Y. Z. Su and X. F. Qian, *J. Power Sources*, 2012, **202**, 230.
47 H. L. Wang, L. F. Cui, Y. A. Yang, H. S. Casalongue, J. T. Robinson, Y. Y. Liang, Y. Cui and H. J. Dai, *J. Am. Chem. Soc.*, 2010, **132**, 13978.